INTERNATIONAL JOURNAL OF SCIENTIFIC & ENGINEERING RESEARCH, VOLUME 10, ISSUE 12, DECEMBER 2019
ISSN 2229-5518

ANALYTICAL MODEL FOR ANTI-CORROSIVE COATING FOR SUBSEA SYSTEMS

Ogunlere Olayinka, Franklin Okoro

ABSTRACT

Similar to every subsea system, anticorrosive coatings require to be designed for optimum durability and performance since intervention in deep waters is highly economically and technically unviable. A very important part of the design of coating systems is in choosing a material that yields optimum corrosion protection performance. For decades, coating material selection greatly depends on the outcomes of experimental aging investigations. However, the impacts of the coating material features on the investigation results require to be understood so as to correctly analyze and optimize the outcomes. This paper which focused mainly on single layer anticorrosive coatings gives a fracture analysis of coating systems with the aim of evaluating the effects of the coating thickness, material features, etc. on its vulnerability to fracture associated failures. A design methodology which is very simple in application was developed to choose the suitable coating thickness to avoid failures as a result of layer cracking, interface delamination, buckle driven debondment and blistering. A fracture toughness utilization factor was applied to define the susceptibility of coating layers to specific failure modes. The evaluation gave the maximum allowable thicknesses for a fusion bonded epoxy coating, a polyetherimide coating and a polyamide-12 coating within pre-specified limits. From the outcomes, the fusion bonded epoxy coating is the most appropriate of the three coatings for subsea usage. Further works to enhance the toughness of the fusion bonded epoxy coating to layer cracking revealed that the addition of minerals or glass fillers to the epoxy coating greatly enhances its long term corrosion protection performance.

Keywords: Corrosion, Coating, Subsea Systems, Fracture, Materials.

Ogunlere Olayinka is a post graduate student of Offshore Technology Institute, UNIVERSITY OF PORT-HARCOURT. Email: ogunlere.olayinka@gmail.com

Franklin Okoro is the Group Coordinator of CLEANSCRIPT GROUP, a research company in Nigeria. Email: f.obiohaokoro@gmail.com

2. INTRODUCTION

Surface corrosion control is arguably the most important design consideration made for most deepwater systems. This destructive phenomenon which can either be general or localized poses a huge risk to both the continuous and long term use of deep water assets, and the safety of offshore personnel.

Following the definitions of the National Association of Corrosion Engineers, general corrosion is usually uniformly distributed over the material surface whereas localised corrosion is restricted to a small area of the corroding surface [1]. While general corrosion causes a uniform loss of wall thickness and resultant degradation of a subsea system,

INTERNATIONAL JOURNAL OF SCIENTIFIC & ENGINEERING RESEARCH, VOLUME 10, ISSUE 12, DECEMBER 2019
ISSN 2229-5518

localised corrosion poses a higher damaging threat because it can go through the wall thickness of a system and cause loss of containment of produced fluids or give rise to an initiation point for stress corrosion cracking of the system.

As a result of this, the need for a reliable corrosion preventive measures through the design life of a subsea system so as to mitigate against corrosion related failures cannot be overemphasized. For a permanent submerged system, the widely adopted industry practice for corrosion control is a combination of compatible anti-corrosion coatings and cathodic protection which can either be active or passive. Coatings are generally seen as the first line of protection against surface corrosion while the cathodic protection acts as a redundancy or fail safe to the anti-corrosion coating system in case the coating gets affected in any way [2].

The effect of corrosion on the reliability and efficiency of subsea systems, and even on the availability of funds for future projects calls for a very thorough and conservative measures for corrosion control and mitigation. For minimum levels of subsea corrosion to be achieved, [3] propose a detailed assessment of the degree of existing corrosion damage as the major factor for choosing suitable corrosion control measures to be applied. This method being an inspection approach strategy is very viable especially when proactively applied to develop predictive maintenance measures for corrosion prevention. However, its implementation on subsea systems is unviable owing to the fact that the maintenance of coating and cathodic protection systems for subsea systems is largely impracticable. The cost and time effects would be very unimaginably colossal even if it were possible to maintain deep water assets. Because of this, corrosion management for deepwater applications is characterised by a very high need for quality control of the control measures to be deployed [4].

A very important part of the corrosion protection system used for most deepwater systems is the anti-corrosive coating system which serves as the first line of defence by physically protecting the vulnerable deepwater systems from the corrosive environment. For coating systems that are deployed together with cathodic protection, the needed current density and associated cost of efficient corrosion protection is largely reduced because of the application of the coating. The degree of current density reduction as a result of the application of coating is usually referred to as the coating breakdown factor and it depends on certain factors such as coating characteristics, operational parameters and time [5]. For the coating breakdown and the cathodic protection current requirement to be minimized, coatings are usually designed for a long duration integrity

INTERNATIONAL JOURNAL OF SCIENTIFIC & ENGINEERING RESEARCH, VOLUME 10, ISSUE 12, DECEMBER 2019
ISSN 2229-5518

assurance throughout the design life of the system to be protected. Normally, anti-corrosion coatings are needed to satisfy and meet many subsea system operational requirements such as high mechanical strength and good ageing resistance [6].

Therefore, the optimum design of the corrosion protection system for a given application will require the accurate choice and implementation of corrosion protection coatings in order to reduce the cathodic protection needs and improve its efficiency. Also, the optimum design of the corrosion protection coating against early failure needs an understanding of its anti-corrosive potentials and the mode of failure in order to provide a basis for the design. Currently, anti-corrosive performance testing is generally deployed for the aim of comparison and grading of protection coatings as well as removing coatings likely to fail too early [7]. An assessment of performance tests for deepwater anti-corrosive coatings is provided by Mitchell, et al (2005) [8]. Though the basic anti- corrosive performance tests accurately assess and compare several coatings' performance, a quantitative assessment gives an added advantage of ease of re-creation and optimization of the results. This paper therefore targeted a quantitative assessment of the mechanical integrity of anti-corrosive coatings so as to minimize the probability of premature coating failures as a result of mechanical stresses.

3. METHODOLOGY

ANALYSIS OF MECHANICAL FAILURE AND COATING SYSTEMS DESIGN

Mechanics of Fracture in Design

Fracture analysis is carried out usually by two methods: the intensity of stress method and the energy balance method.

The Energy Balance Method

For a crack in a solid structure to extend in length, an adequate quantity of potential energy is needed to overpower the surface energy of the material. The entire energy in connection with crack growth can be connoted as:

$$U_T = U_P + U_E + U_S \quad (3.1a)$$

where U_T is the total energy, U_P is the potential energy provided by an external load energy, U_E is the elastic strain energy in the elastic channel which depends on the crack profile and $U_S = \Gamma A$ is the surface energy having Γ as the distinct surface energy of the material and A is the crack area. From Griffith's energy principle, unconstrained fracture happens if these criteria are met:

$$dU_T = dU_P + dU_E + dU_S \leq 0. \quad (3.1b)$$

The energy dissipation rate is known as the rate of the energy available for an extension of the crack. It is basically the 'crack extension strength'. Numerically, the energy

INTERNATIONAL JOURNAL OF SCIENTIFIC & ENGINEERING RESEARCH, VOLUME 10, ISSUE 12, DECEMBER 2019
ISSN 2229-5518

dissipation rate, G is the measure of the variation in potential energy as a result of both elastic strain and external force with the crack area as expressed below:

$$G = -\left(\frac{dU_P}{dA} + \frac{dU_E}{dA}\right). \quad (3.2)$$

By inputting equation (3.2) into equation (3.1b), the crack growth principle can be given in terms of the energy dissipation rate as:

$$(G - \Gamma)dA \geq 0. \quad (3.3)$$

Hence, the critical point for the onset of unconstrained fracture can be expressed mathematically as:

$$G = \Gamma. \quad (3.4)$$

For a fractured solid structure, the distinct surface energy, Γ is the rate of the fracture resistance of the material while for a fractured contact surface between two interconnected materials, Γ expresses the distinct surface adhesion between the two layers.

The Stress Intensity Method

There are three popular means by which a crack may be loaded, as illustrated in Figure 3.1. Typically, the stress intensity parameter is assigned a subscript to represent the means of loading, i.e., K_I, K_{II} or K_{III}.

If a polar axis of ordinates with the onset of the crack tip is known, the stress fields before a crack tip in an identical linear elastic material can be expressed for Modes I, II and III as:

$$\lim_{r\to 0} \sigma_{ij}^{(I)} = \frac{K_I}{\sqrt{2\pi r}} f_{ij}^{(I)}(\theta) \quad (3.5a)$$

$$\lim_{r\to 0} \sigma_{ij}^{(II)} = \frac{K_{II}}{\sqrt{2\pi r}} f_{ij}^{(II)}(\theta) \quad (3.5b)$$

$$\lim_{r\to 0} \sigma_{ij}^{(III)} = \frac{K_{III}}{\sqrt{2\pi r}} f_{ij}^{(III)}(\theta) \quad (3.5c)$$

where σ_{ij} = stress tensor,

r and θ are as shown in Figure 3.2,

K_I, K_{II} and K_{III} = Modes I, II and III stress intensity parameters respectively,

$f_{ij}^{(I)}$, $f_{ij}^{(II)}$ and $f_{ij}^{(III)}$ = dimensionless functions of θ.

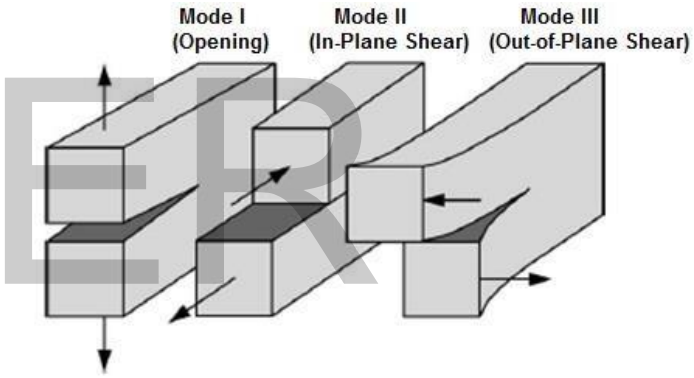

Figure 3.1: The three means of loading that can be implemented to a crack [18]

As shown in Equation (3.5), the stresses close to the crack tip varies proportionally to K. Therefore, if K is defined, it is feasible to solve for all elements of stress with respect to r and θ. In a mixed mode condition, the individual impact of the different loading modes to a specific stress element are additive as below;

INTERNATIONAL JOURNAL OF SCIENTIFIC & ENGINEERING RESEARCH, VOLUME 10, ISSUE 12, DECEMBER 2019
ISSN 2229-5518

$$\sigma_{ij}^{(total)} = \sigma_{ij}^{(I)} + \sigma_{ij}^{(II)} + \sigma_{ij}^{(III)} \quad (3.6)$$

With equation (3.6), a crack on a linear elastic material will grow spontaneously if the entire stress is more than the peak allowable stress which is a measure of the material's fracture resistance.

For a crack in a material with Young's modulus, E and Poisson's ratio ν, the correlation between the energy dissipation rate, G and the stress intensity parameter is (Hutchinson & Suo, 1991):

$$G = (K_I^2 + K_{II}^2)\frac{(1-\nu^2)}{E} \quad (3.7)$$

Layer cracking

When the film surface materials and their surface contacts give in to variations in temperature in an elastic way, a biaxial misfit stress can be correlated accordingly as:

$$\sigma^T = (\alpha_f - \alpha_s)(T_R - T_r)\, E_f/(1-\nu_f) \quad (3.8)$$

where α_f and α_s are the coefficients of thermal expansion for the coating film and the surface respectively, T_R is the reference temperature at which the film/surface system is 'thermally' stress-free, T_r is the room temperature, E_f and ν_f are the coating films Young's modulus and Poisson's ratio respectively. The biaxial misfit stress, σ^T here represents residuary stresses in the coating layer just because of thermal mismatch between the coating and substrate materials and the temperature variations during the coating laying process.

The basic correlation for the steady-state average energy dissipation rate over the extension front of a semi-boundless inaccessible crack is given as:

$$G_{ss} = \frac{\pi\left(1-\nu_f^2\right)\sigma^2 h}{2E_f} f(D_\alpha, D_\beta) \quad (3.9)$$

where h is the film layer thickness, E_f and ν_f are the coating film's Young's modulus and Poisson's ratio respectively, σ is the homogenous prestress in the coating film that is perpendicular to the crack line. The Dundur's parameters, D_α and D_β are dimensionless integration of elastic moduli which distinguishes the elastic mismatch between the coating film and the metal surface and are given by:

$$D_\alpha = \frac{\bar{E}_f - \bar{E}_s}{\bar{E}_f + \bar{E}_s}$$ and

$$D_\beta = \frac{1}{2}\frac{\mu_f(1-2\nu_s) - \mu_s(1-2\nu_f)}{\mu_f(1-\nu_s) + \mu_s(1-\nu_f)} \quad (3.10)$$

where E_s and ν_s are the surface Young's modulus and Poisson's ratio respectively,

$\mu_i = \frac{E_i}{2(1+\nu_i)}$ and $\bar{E}_i = \frac{E_i}{(1-\nu_i^2)}$ is the shear modulus and plane strain tensile modulus respectively for $i = \{f, s\}$.

The criteria for growth of an inaccessible crack over the coating film is given as:

$$G_{ss} = \Gamma_c \quad (3.11)$$

INTERNATIONAL JOURNAL OF SCIENTIFIC & ENGINEERING RESEARCH, VOLUME 10, ISSUE 12, DECEMBER 2019
ISSN 2229-5518

where Γ_c is the mode-I fracture resistance of the coating film with units of energy per unit area.

Surface Contact Delamination

A model of an unstable surface contact under relatively general loading conditions is illustrated in Figure 3.2. Each material is presumed to be isotropic and linearly elastic. The layers of the coating film and the metal surface are denoted as h and H respectively.

Prior to the edge of the crack, the film/surface system may be seen as a blended beam with its unaligned axis at a distance $h\Delta$ up of the bottom of the beam, with Δ correlated as

$$\Delta = \frac{1 + 2\Sigma\eta + \Sigma\eta^2}{2\eta(1 + \Sigma\eta)}, \quad (3.12)$$

where $\Sigma \equiv \frac{1 + D_\alpha}{1 - D_\alpha}$ and $\eta = \frac{h}{H}$. (3.13)

The non-dimensional cross-sectional area, A and moment of inertia, I of the blended beam are:

$$A = \frac{1}{\eta} + \Sigma, \quad I = \Sigma\left[\left(\Delta - \frac{1}{\eta}\right)^2 - \left(\Delta - \frac{1}{\eta}\right) + \frac{1}{3}\right] + \frac{\Delta}{\eta}\left(\Delta - \frac{1}{\eta}\right) + \frac{1}{3\eta^3}$$

(3.14)

The energy dissipation rate can be estimated by taking the variation between the energy within the system per unit length before and after the edge of the crack and is given as:

$$G = \frac{1}{2\bar{E}_f}\left(\frac{P_1^2}{h} + 12\frac{M_1^2}{h^3}\right) + \frac{1}{2\bar{E}_s}\left(\frac{P_2^2}{H} + 12\frac{M_2^2}{H^3} - \frac{P_3^2}{Ah} - \frac{M_3^2}{Ih^3}\right)$$

(3.15)

The critical point of the energy dissipation rate for surface contact fracture, also referred to as the resistance of the surface contact can be termed as an effectual substrate energy which is dependent on the loading mode. The degree of relative mode-II to mode-I loading (mode mixity) at the surface contact is determined by the phase angle ψ and is given as:

$$\psi = \tan^{-1}(K_{II}/K_I). \quad (3.16)$$

Equation (3.16) usually denotes the mode mixity when D_β is zero. But, it is also a fairly good correlation when $D_\beta \neq 0$ because the impacts of small nonzero values of D_β are not pronounced in most cases [9].

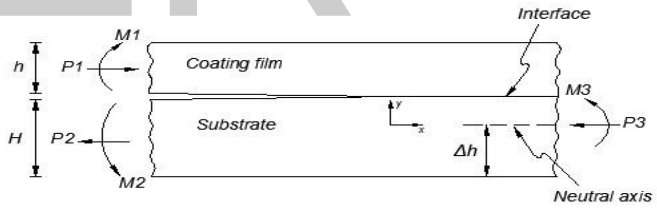

Figure 3.2: An illustration of an interface crack [11]

As can be seen from equation (3.14), a phase angle of $\psi = 0°$ means a uniform mode-I loading whereas a phase angle of $\psi = 90°$ implies a uniform mode-II loading. For the surface contact crack issue explained above, the phase angle, ψ is given as:

$$\psi = \tan^{-1}\left[\frac{\lambda\sin\omega - \cos(\omega+\gamma)}{\lambda\cos\omega + \sin(\omega+\gamma)}\right] \quad (3.17)$$

INTERNATIONAL JOURNAL OF SCIENTIFIC & ENGINEERING RESEARCH, VOLUME 10, ISSUE 12, DECEMBER 2019
ISSN 2229-5518

where λ assesses the loading mixture as

$$\lambda = \sqrt{\frac{V}{U}}\frac{Ph}{M} \quad (3.18)$$

where P and M are linear mixtures of the crack tip loads:

$$P = P_1 - C_1P_3 - C_2M_3/h, \qquad M = M_1 - C_3M_3. \quad (3.19)$$

The geometric parameters are defined by:

$$C_1 = \frac{\Sigma}{A}, \quad C_2 = \frac{\Sigma}{I}\left(\frac{1}{\eta} + \frac{1}{2} - \Delta\right), \quad C_3 = \frac{\Sigma}{12I} \quad (3.20)$$

and by

$$U = \frac{1}{1 + \Sigma\eta(4 + 6\eta + 3\eta^2)}, \quad V = \frac{1}{12(1 + \Sigma\eta^3)} \quad (3.21)$$

$$\sin\gamma = 6\Sigma\eta^2(1 + \eta)\sqrt{UV}. \quad (3.22)$$

All the correlations have been developed based on the traditional beam theory. The angle ω is varies with Dundur's parameters D_α, D_β and relative height η. Suo & Hutchinson (1990) [10] gave a robust tabulation of the parameter ω after solving the elasticity problem mathematically.

The condition for the onset of crack propagation in the surface contact when the edge of the crack is loaded is defined as:

$$G = [1 + (1 - \rho)\, tan^2\psi], \quad (3.23)$$

where Γ_i is the uniform mode-I resistance of the surface contact and the factor ρ varies the effect of the mode-II impact in the condition. The limit $\rho = 1$ is the 'typical brittle' surface contact with a surface contact crack onset occurring at $G = \Gamma_i$ for all mode mixtures.

A typical example of a surface contact delamination issue is that of surface contact cracks in pretensioned films because of border defects or channels in the coating film. For this issue, the misfit stress, σ in the coating film because of the film deposition is equal to the mechanical loads:

$$P_1 = P_3 = \sigma h, \qquad M_3 = (1/2 + 1/\eta - \Delta)\,\sigma h^2, \qquad M_1 = 0. \quad (3.24)$$

It is worthy of note that the net equilibrium of the surface contact crack model gives the following equilibrium limitations among the six load factors:

$$P_1 - P_2 - P_3 = 0, \quad (3.25a)$$

$$M_1 - M_2 + P_1(h/2 + H - h\Delta) + P_2(h\Delta - H/2) - M_3 = 0. \quad (3.25b)$$

Inputting equations (3.22) and (3.23) into equation (3.13) results to the elaborate energy dissipation rate for a surface contact crack in a pretensioned film because of border defects or channels:

$$G = \frac{\sigma^2 h}{2\bar{E}_f}\left[1 - \frac{\Sigma}{A} - \frac{\Sigma}{I}\left(\frac{1}{\eta} + \frac{1}{2} - \Delta\right)^2\right]. \quad (3.26)$$

The Straight-sided Blister (one dimensional blister)

Assume a parameter 'x'–independent section of a linear-sided blister defined by y – and z – displacements as shown in Figure 3.3, for which the coating film is not adjoined to the surface in the strip area $-b \le y \le b$. The surface is here assumed to be limitlessly thick.

The unbent film is assumed to being under the influence of a pure, equi-biaxial compressive internal stress, $\sigma_{xx} = \sigma_{yy} = \sigma$.

INTERNATIONAL JOURNAL OF SCIENTIFIC & ENGINEERING RESEARCH, VOLUME 10, ISSUE 12, DECEMBER 2019
ISSN 2229-5518

The magnitude of the bending or buckling, ξ has been characterized such that the central buckling deflection, δ is equal to ξh. It is correlated to the residuary stress in the coating film by:

$$\xi = \left[\frac{4}{3}\left(\frac{\sigma}{\sigma_c} - 1\right)\right]^{1/2}, \quad (3.27)$$

where σ_c is the traditional buckling stress of a clamped-clamped wide plate and is defined by:

$$\sigma_c = \frac{\pi^2}{12}\frac{E_f}{\left(1-\nu_f^2\right)}\left(\frac{h}{b}\right)^2. \quad (3.28)$$

As can be seen from equation (3.25), the residuary compressive stress in the film, σ must be more than the traditional buckling stress, σ_c if the film is to bend away from the surface for a known surface contact crack extension '$2b$'. The energy dissipation rate and phase angle for the linear-sided blister issue have been defined respectively by Hutchinson & Suo (1991) [11] as:

$$G = [(1 - {}^{2})h/(2E_f)](\sigma - \sigma_c)(\sigma + 3\sigma_c), \quad (3.29)$$

and

$$\tan\psi = \frac{4\cos\omega + \sqrt{3}\,\xi\sin\omega}{-4\sin\omega + \sqrt{3}\,\xi\cos\omega}. \quad (3.30)$$

Here, $\omega = (D_\alpha, D_\beta, \eta = 0)$

In the same way as the previous case of a surface contact crack, the condition for a stable extension of the one-dimensional linear-sided blister is defined as:

$$G = [1 + (1 - \rho)\,tan^2\psi] \quad (3.31)$$

The Circular Blister

The profile for the circular blister is same as that in Figure 3.3 besides the radius of the buckled region which is taken as R. The correlation for circular blisters as proposed by Hutchinson & Suo (1991) [11] are presented below:

The traditional bending stress of a clamped circular plate is

$$\sigma_c^* = 1.2235\frac{E_f}{\left(1-\nu_f^2\right)}\left(\frac{h}{R}\right)^2. \quad (3.32)$$

The magnitude of the bending deflection, ξ is given as

$$\xi = \left[\frac{1}{c_1}\left(\frac{\sigma}{\sigma_c^*} - 1\right)\right]^{1/2}, \quad (3.33)$$

where

$$c_1 = 0.2473\,(1 + \nu_f) + 0.2231(1 - \nu_f^2). \quad (3.34)$$

The energy dissipation rate and phase angle for the circular blister issue were defined by Hutchinson & Suo (1991) [11] and are presented as:

$$G = \frac{(1-\nu_f)h\sigma^2/E_f}{[1+0.9021(1-\nu_f)]}\left[1 - \left(\frac{\sigma_c^*}{\sigma}\right)^2\right] \quad (3.35)$$

and

$$\tan\psi = \frac{\cos\omega + 0.2486(1+\nu_f)\,\xi\sin\omega}{-\sin\omega + 0.2486(1+\nu_f)\xi\cos\omega}. \quad (3.36)$$

with $\omega = \omega(D_\alpha, D_\beta, \eta = 0)$

The condition for a stable extension of the circular blister is presented as:

$$G = [1 + (1 - \rho)\,tan^2\psi] \quad (3.37)$$

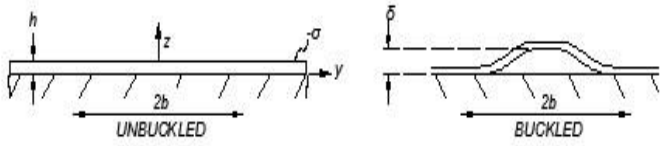

Figure 3.3: Profile of a one-dimensional blister. Left: unbent; Right: bent; [11]

Osmotic Blistering

For a thin blister layer h as illustrated in Figure 3.4, if a fluid pressure p_i acts underneath the membrane while an external pressure p_e such as a hydrostatic pressure acts on the other side, a net pressure variation $p = p_i - p_e$ acts on the blister.

The central deflection, δ and the volume beneath the blister, V are respectively given as:

$$\delta = A_1 \left(\frac{pR^4}{E_f h}\right)^{1/3}, \quad \text{and} \quad V = A_2 \pi R^2 \delta, \tag{3.38}$$

where E_f is the coating film's Young's modulus, R is the delamination or deboning radius, $A_1 = 0.662$ for Poisson's ratio $\nu_f = 0.3$ and $A_1 = 0.595$ for Poisson's ratio $\nu_f = 0.5$, $A_2 = 0.518$ for Poisson's ratio $\nu_f = 0.3$ and $A_2 = 0.519$ for Poisson's ratio $\nu_f = 0.5$.

If the pressure beneath the blister is assumed to be constant and acting homogenously over the total blister area, then the mechanical energy release rate or crack advancing force because of the applied fluid pressure can be defined as:

$$G = \frac{5A_1A_2}{4}\left(\frac{1}{E_f h}\right)^{1/3}(pR)^{4/3} \tag{3.39}$$

From equation (3.36), the formula for the mechanical energy dissipation rate can be given as:

$$G = \frac{5A_2}{4} p\delta. \tag{3.40}$$

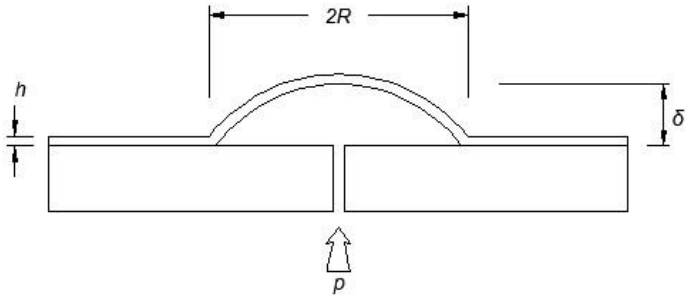

Figure 3.4: Illustration of a pressurized blister acted on by constant pressure [12].

In another work on the fracture analysis of a blister test to define the toughness of coating films to sudden surface contact fracture as a result of the action of osmotic pressure, Hutchinson & Suo (1991) [11] defined the central deflection of the blown up blister as:

$$\delta = \frac{1}{64} pR^4/D, \tag{3.41}$$

where D is the buckling stiffness of the coating film defined as

$$D = \frac{E_f h^3}{12(1-\nu_f^2)}. \tag{3.42}$$

Inputting equation (3.40) into equation (3.39) results to:

$$\delta = \frac{3}{8}\frac{\left(1-\nu_f^2\right)pR^4}{E_f h^3}, \tag{3.43}$$

Hutchinson & Suo (1991) [11] defines the mechanical energy release rate of a blown up blister as

INTERNATIONAL JOURNAL OF SCIENTIFIC & ENGINEERING RESEARCH, VOLUME 10, ISSUE 12, DECEMBER 2019
ISSN 2229-5518

$$G = \frac{8}{3}\frac{E_f h^3 \delta^2}{(1-\nu_f^2)R^4} = p\delta \quad (3.44)$$

From equations (3.38) and (3.42), it is evident that the energy release rate as proposed by Wan & Mai (1995) [12] is approximately 35% less than the energy release rate proposed by Hutchinson & Suo (1991) [11]. The phase angle of the inflated blister by Hutchinson & Suo (1991) [11] is defined as:

$$\tan\psi = -\cot\omega. \quad (3.45)$$

Coating System Design

From the earlier analysis, it can be seen that for a constant radius of an inflated blister, the pressure, p the blister layer can resist is highly dependent on the coating layer thickness, h. That is to say that the thicker the coating layer, the more pressure it can resist for a known blister radius. However, increasing the thickness of the coating layer increases its vulnerability to layer cracking, surface contact delamination and buckle driven debond as a result of excessive in-plane stresses in the coating layer. Therefore, the choice of the thickness of the coating layer can be an optimization problem which can be solved as follows:

$$Maximize\ p^{(final)} = FTU \times \left[\Gamma_i(\psi)^{(final)} \times \frac{8}{3}\frac{E_f^{(final)} \times h^3}{\left(1-\nu_f^2\right)R^4}\right]^{1/2} \quad (3.46a)$$

$$subject\ to$$

$$G(h)^{(initial)}_{(layer\ cracking)} \leq FTU \times \Gamma_c^{(initial)} \quad (3.46b)$$

$$G(h)^{(initial)}_{(interface\ debond)} \leq FTU \times \Gamma_i(\psi)^{(initial)} \quad (3.46c)$$

$$G(h)^{(initial)}_{(buckle\ driven\ delamination)} \leq FTU \times \Gamma_i(\psi)^{(initial)} \quad (3.46d)$$

$$h_{min} \geq h \geq h_{max}. \quad (3.46e)$$

where the superscripts 'initial' and 'final' denotes the state of the coating system upon deposition and at the end of its service life respectively, FTU represents 'fracture resistance utilization' which is primarily the ratio of the crack driving force G to the useful fracture resistance $\Gamma_i(\psi)$ or Γ_c. An allowable fracture resistance utilization could be given beforehand as a safety factor to avoid fracture failures. The parameters h_{min} and h_{max} in equation (3.46e) represents the standard minimum and maximum coating film thicknesses respectively. The subscripts 'layer cracking', 'interface debond' and 'buckle driven delamination' in equation (3.46) were just used to show the specific mode of failure as a result of the associated energy release rates.

Design Assumptions

- Both the surface and the coating are isotropic and linearly elastic.

INTERNATIONAL JOURNAL OF SCIENTIFIC & ENGINEERING RESEARCH, VOLUME 10, ISSUE 12, DECEMBER 2019
ISSN 2229-5518

- The impacts of innate residuary stresses in the coating film are minimal during deposition. The residuary stresses are mainly as a result of thermal mismatch.
- Blister growth is mainly due to the action of the fluid pressure underneath the blister. The impacts of internal residual stresses in the coating film are taken to be minimal as the blister grows.

4. RESULTS AND DISCUSSION

Initial Data

Table 4.1: Material characteristics of a common epoxy coating system [13].

Property	Epoxy Coating	Steel Surface
Young's Modulus [GPa]	3.83	200
Poisson's ratio [-]	0.33	0.3
Coefficient of thermal expansion [μstrain]	33.7	Not available
Glass transition temperature [°C]	140	Not applicable

Sue & Chang (2006) [13] experimentally studied the gluing strength of a fusion bonded epoxy (FBE) coating on a steel surface and provided the facts as shown in Table 4.1. In Sue and their experiment, it was discovered that for a surface layer of 3mm, the FBE/Steel surface contact had a uniform mode-I surface contact fracture resistance of 1.1kJm^{-2}. Three identical FBE coating tests having thicknesses of 4mils, 8mils and 12mils were all discovered to have dry adhesive durability over 50MPa which dropped by approximately 60 – 80% during a wet delamination test set up by NACE TM0304 standard for investigating the deterioration of coating's wet adhesion durability. The mode-I fracture strength of the surface contact was as well discovered to deteriorate by approximately 60% in the course of the wet delamination test.

In a different study, Lau (2011) [14] found that the impact of wetness on structural epoxy is damaging with a reduction in surface contact fracture strength of over fifty percent. From these outcomes, an approximation of a 60% reduction in adhesion and/or surface contact mode-I fracture strength as a result of long term submersion of an epoxy coating would be normal.

Besides FBE coatings, other anticorrosive coatings to be evaluated in this study include Polyetherimide (PEI) and Polyamide 12 (PA-12) which have been studied comparatively on their corrosion protection strength by Lima, et al. (2013). The features of both the PEI and Polyamide coatings on a steel surface as provided by Lima, et al. (2013) [15] are shown in Table 4.2

INTERNATIONAL JOURNAL OF SCIENTIFIC & ENGINEERING RESEARCH, VOLUME 10, ISSUE 12, DECEMBER 2019
ISSN 2229-5518

Table 4.2: Features of common PEI and Polyamide 12 coating system

Property	**PEI**	**Polyamide 12**
Adhesion [MPa]	**9.0 ± 1**	**11.2 ± 1.2**
Coefficient of thermal expansion [µstrain]	**21**	**111**
Glass transition temperature [°C]	**216**	**37**

The mode-I fracture strength for the PEI/Steel and Polyamide/Steel surface contacts have been instinctively assumed to be within the ranges of 200 – 250 J/m² and 250 – 300J/m² respectively based on the approximation that the dry adhesive durability of a polymer surface contact varies directly with its surface contact fracture strength.

Other material features required for the fracture evaluation in this study can be gotten from CES EduPack (2018) [16] and are provided in Table 4.3:

Table 4.3: Supplementary property data obtained from CES EduPack [16].

Property	PEI	Polyamide 12	FBE	Steel Substrate
Young's Modulus [GPa]	2.98 – 3.04	0.35 – 0.42	-	-
Poisson's ratio [-]	0.385 – 0.401	0.406 – 0.422	-	-
Coefficient of thermal expansion [µstrain]	-	-	-	11.5 – 12.5
Mode-I fracture toughness [MPa.m$^{1/2}$]	1.99 – 4.03	2.6 – 2.7	0.4 – 0.7	43 - 63

The data as provided in Tables 4.1 and 4.2 were results from experimental investigations which are published in reputable journals and are considered significantly accurate and reliable, while the data provided in Table 4.3, though fairly reliable gives very little or no exactness or accurateness because they are only upper and lower limits. These data together with other data approximations and assumptions earlier stated have been used to reveal a comparative

INTERNATIONAL JOURNAL OF SCIENTIFIC & ENGINEERING RESEARCH, VOLUME 10, ISSUE 12, DECEMBER 2019
ISSN 2229-5518

evaluation of the selected anticorrosive coatings based on their corrosion performance. It is important to note here that the outcomes from this study as shown in the following sections are more illustrative and descriptive than informative and should only be utilised critically, so that the outcomes can be validated or modified.

Coating residuary internal stress

The analysis of the residual internal stresses built in the coating thickness upon deposition is the focus of this section. The thermal mismatch stress between individual coating and the steel surface is estimated using equation (3.8) and are provided in Table 4.4. As proposed by Perera (1996) [17], the glass transition temperature is adopted as the reference temperature at which the coating material is 'thermally' stress-free because the coating only loses ductility as it cools below the glass transition temperature.

Table 4.4: Typical coating thermal mismatch stresses

	FBE	**PEI**	**Polyamide - 12**
Young's Modulus [GPa]	3.83	2.98 – 3.04	0.35 – 0.42
Thermal mismatch stress [MPa]	14.2	8.54 – 8.71	0.71 – 0.85

Comparative evaluation of the coatings' vulnerability to layer cracking and interface delamination

Layer cracking

Because the exact values of mode-I fracture strength and Young's modulus of the coatings are not available, the fracture strength/toughness utilization, which is the ratio of energy release rate to fracture strength of individual coatings is analyzed at limit conditions to define its upper and lower possible values over a range of coating thicknesses as illustrated in Figure 4.1.

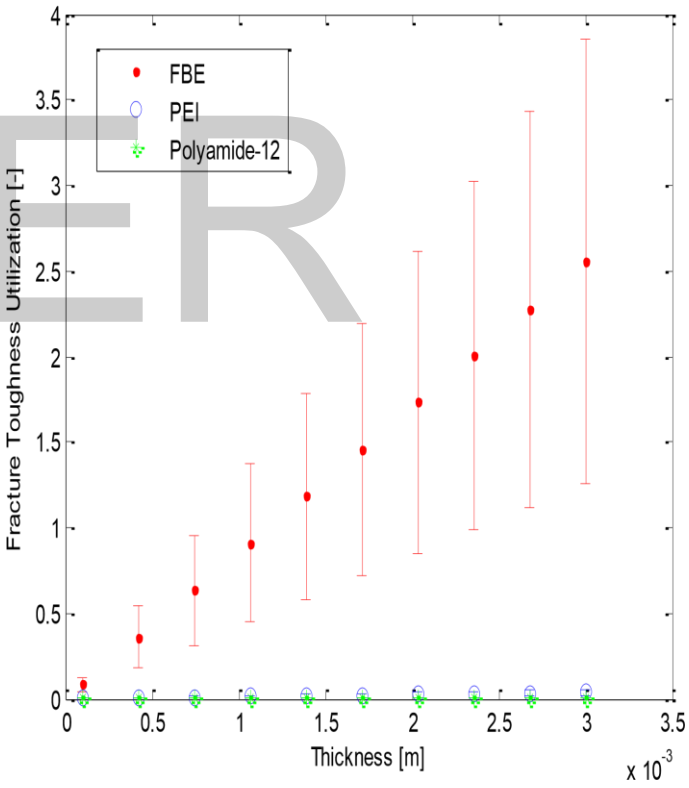

Figure 4.1: Evaluation of coating vulnerability to layer cracking

INTERNATIONAL JOURNAL OF SCIENTIFIC & ENGINEERING RESEARCH, VOLUME 10, ISSUE 12, DECEMBER 2019
ISSN 2229-5518

The range bars in Figure 4.1 reveal the maximum and minimum limits of fracture toughness utilization for all practicable combinations of Young's modulus and mode-I fracture strength within the ranges showed in the initial data section. In spite of the doubts as a result of lack of precision, it is obvious that the fracture toughness utilization of the FBE coating was very fast to approach unity than the other two coatings. A fracture toughness utilization of unity means that the steady state energy release rate in connection with a through thickness crack in the coating layer is equal to the fracture strength of the material and the material is susceptible to spontaneous layer cracking or channeling.

The high values of fracture toughness utilization observed for FBE are clearly as a result of the huge thermal loads exerted on the FBE coating in contrast with the other two coatings. Based on the outcomes presented in Figure 4.1, if there is a through thickness crack in the FBE coating of film thickness above 800μm, the coating becomes prone to fast fracture and channeling cracks on the coating substrate. Though, practically the upper or peak allowable thickness for the FBE coating would be less because the internal residuary stress in the coating layer may be higher because of the additional innate tensile loads due to the deposition process. This outcome is in harmony with the acceptance **of** about 600μm thick FBE coatings as high thickness monolayer coatings by the industry [6].

Surface Contact/Interface Delamination

The probability of the coatings to delaminate as a result of tensile residual loads and stresses exerted during the process of deposition is also evaluated based on the coating/steel surface contact fracture toughness utilization. Figures 4.2a and 4.2b respectively illustrate the estimated bounds for the surface contact fracture toughness utilization for the entire coating materials at upper and lower mode-II impact on the interface fracture strengths as defined by ρ in equation (3.23).

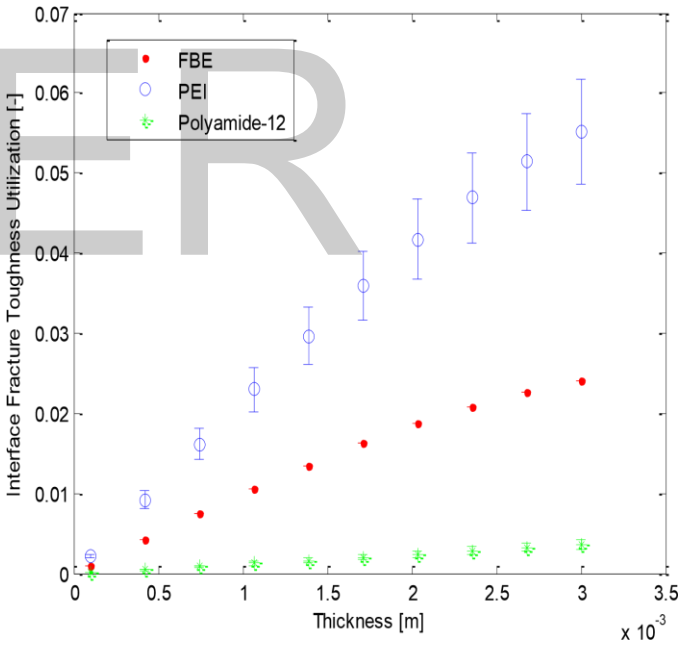

Figure 4.2a: Vulnerability of the coating surface contacts to delamination when the mode-II impact on the interface sstrength is maximum ($\rho = 0$)

INTERNATIONAL JOURNAL OF SCIENTIFIC & ENGINEERING RESEARCH, VOLUME 10, ISSUE 12, DECEMBER 2019
ISSN 2229-5518

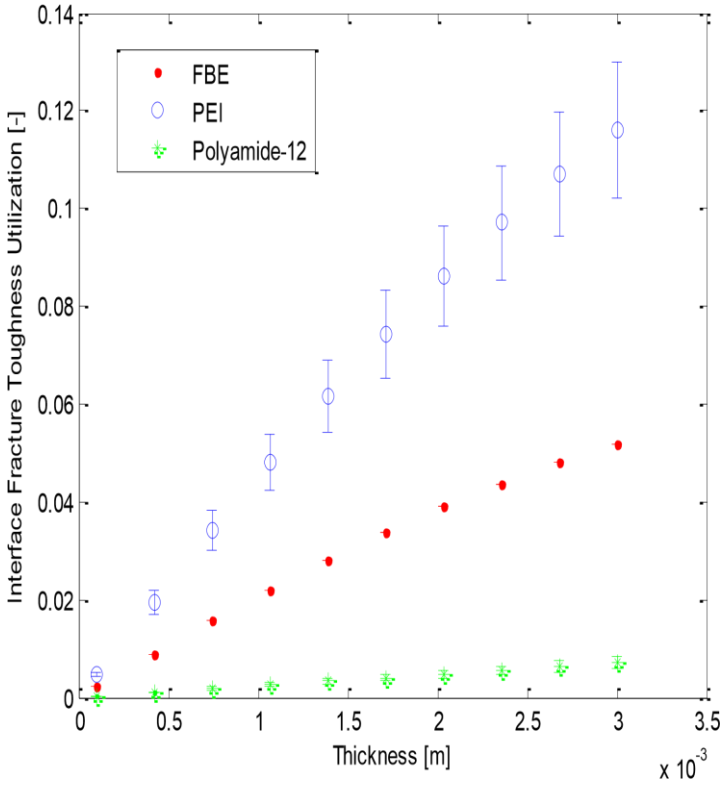

Figure 4.2b: Vulnerability of the coating surface contacts to delamination when the mode-II impacts on the interface strength is minimum (ϱ = 1)

For a surface contact with ρ equals 1, the effective interface strength is equal to the surface contact mode-I fracture strength and the interface is deemed as being essentially brittle. It is seen from Figure 4.2b that even when the surface contacts were quite brittle, the probability of the coating layers to debond from the surface as a result of residual thermal mismatch loads is very low for the entire coating for thicknesses of 3mm and above. However, it is worth to note that the uniform mode-I surface contact fracture strength values assumed for the PEI/Steel and Polymide-12/Steel surface contacts may vary from their real values.

The outcomes provided in Figures 4.2a and 4.2b also show that the characteristics of the coating/surface interface hugely impacts on the surface contact fracture strength and hence the probability of fracture failure at the surface contact. The fracture toughness utilization values observed when the interfaces were assumed to be ideally brittle ($\rho = 1$) are recorded to be approximately 100% more than when the interfaces are deemed less brittle (at $\rho = 0$). Hence, very brittle surface contacts are more possibly to be 'unstable' and risks the reliability of the coating system if the loads on the coating layer become significant under service states. Increasing the surface roughness of the surface may well enhance the states of the surface contact and give a better resistance to in-plane shear stresses, however, there are no ways to determine the degree of surface contact brittleness and no obvious correlation between the surface contact brittleness and the surface properties.

Evaluation of the wet adhesion properties of the coatings approaching the end of their design lives.

Blister evaluation was conducted as part of this work to analyze the strength of the coating systems towards the end of their design lives under submerged states as in the case of subsea applications. From the previous results by Sue &

INTERNATIONAL JOURNAL OF SCIENTIFIC & ENGINEERING RESEARCH, VOLUME 10, ISSUE 12, DECEMBER 2019
ISSN 2229-5518

Chang (2006) [13] and Lau (2011) [14], it is assumed here that the deterioration of the coating materials and surface contacts give rise to about 60% reduction in surface contact mode-I fracture and about 30% reduction in the coating material Young's modulus. Also, the mode-II impact on the interface strength is estimated to be 0.3 and a fracture toughness utilization limit of 0.95 is assumed for all three coatings. The estimated bounds for the peak fluid pressure that can be stored underneath an osmotic blister with a radius of 5mm are plotted in Figure 4.3 for all three coating materials under consideration.

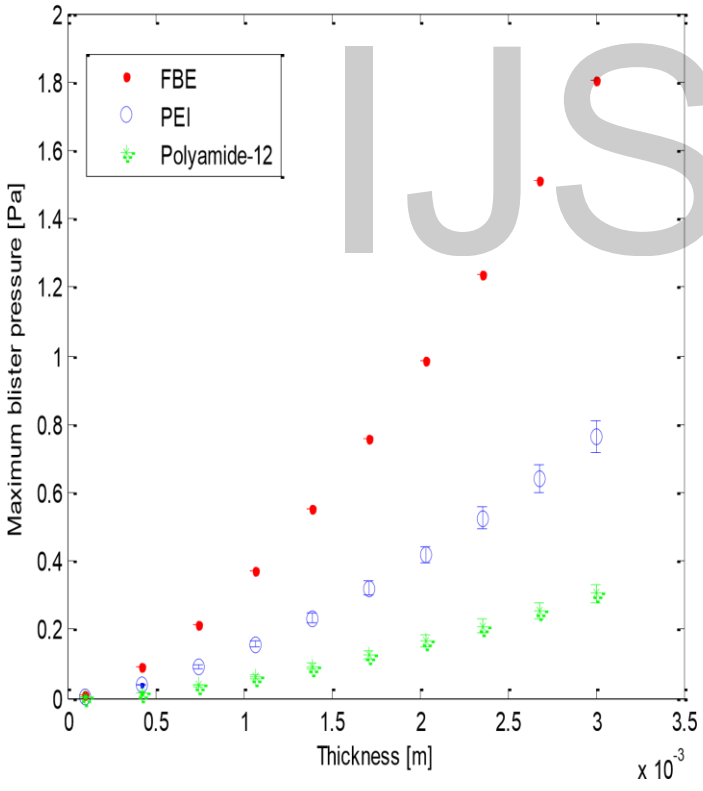

Figure 4.3: Evaluation of coating design life performance based on later life blister analysis

From the results, it is observed that under the same surface contact and blister states, the FBE coating outperforms the other two coatings because the FBE coating has the capacity to overcome approximately twice the size of the maximum blister pressure allowable for the other coatings. In practical, it would even be expected that the likelihood of blister onset in the FBE coating will be far less than that of the PEI and Polyamide-12 coatings because FBE has proven excellent adhesion features and strength to resist water and chemical penetration. Because of this, the PEI and Polyamide 12 coatings if forced to experience submerged corrosion conditions, will most probably face a worse blister condition than an FBE coating for similar duration of submersion time. Summarily, the considered coatings performance was satisfactory with regards to surface contact delamination from edge stresses due to thermal mismatch. All but the FBE coating has excellent resistance to spontaneous layer cracking during coating deposition. Though, the coatings' toughness to wet adhesion deterioration and spontaneous blister growth under submerged conditions is the most important determining factor for the suitability of the coatings for long term subsea coating application. Because of this, the FBE coating is considered to be the most suitable and reliable to be deployed as a single-layer coating for subsea systems since it gives the most efficient long term

INTERNATIONAL JOURNAL OF SCIENTIFIC & ENGINEERING RESEARCH, VOLUME 10, ISSUE 12, DECEMBER 2019
ISSN 2229-5518

resistance against osmotic blistering. However, the possibility of layer cracking with the FBE coating must be addressed to make sure that it is sufficiently reliable.

Enhancing the reliability of the Fusion Bonded Epoxy (FBE) coating.

Enhancements to the reliability of the FBE coating was obtained by the addition of fillers to the epoxy resin with the focus of improving the mechanical features of the coatings. Ranges of relevant mechanical properties of an epoxy with additions as given by CES EduPack (2018) [16] are shown in Table 4.5.

Table 4.5: Mechanical features of filled epoxy [16]

	Glass filled Epoxy	**Mineral filled Epoxy**
Young's Modulus [GPa]	12 – 14	8 – 12
Poisson's ratio [-]	0.32 – 0.36	0.36 – 0.40
Coefficient of thermal expansion [μstrain]	22 – 24	24 – 26
Mode-I fracture toughness [MPa.m$^{1/2}$]	0.8 – 1.1	0.8 – 1.1

Supposedly, the fracture strength of the epoxy coating is improved by the addition of fillers. In contrast with the unfilled epoxy coating (K_{1c} = 0.4 - 0.7 MPa.m$^{1/2}$), it would be anticipated that the filled epoxy coating will give improved resistance to layer cracking. Figure 4.4 shows estimated bounds of fracture toughness utilization for the FBE coatings to analyze their strength against layer cracking as a result of thermal mismatch loads due to the coating deposition process.

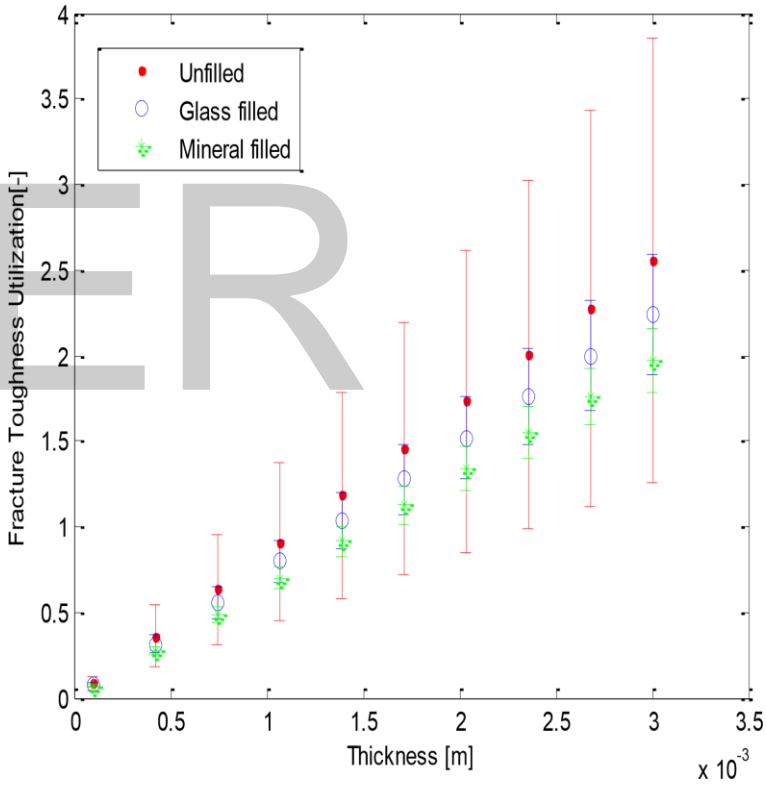

Figure 4.4: Comparative analysis of the vulnerability of different FBE coatings to layer cracking

As anticipated, the addition of fillers to the epoxy resin enhances its strength to withstand layer cracking due to

INTERNATIONAL JOURNAL OF SCIENTIFIC & ENGINEERING RESEARCH, VOLUME 10, ISSUE 12, DECEMBER 2019
ISSN 2229-5518

thermal mismatch loads. From the middle values in each range, it is observed that for similar thicknesses, the mineral filled epoxy coating has a fracture toughness utilization less than that recorded for the glass filled epoxy and the unfilled epoxy. It can also be observed that under the effects of internal residuary loads from thermal mismatch during the process of coating deposition, the presence of a through thickness crack in the mineral filled FBE coating will not probably lead to a spontaneous fracture at thicknesses of 1.1mm or more.

An investigation of the coatings' elastic mismatch defined by the Dundur's parameters shows that the filled coatings are less compliant compared to the unfilled coating on the surface. Thus, the effect of this variation on the interface strength to resist/withstand fracture has to be evaluated to make sure that the coating system does not experience any damaging effects at the surface contact as a result of the addition of fillers. Anyways, the variations in heights of the range bars as seen in Figure 4.4 is because of the input data ranges and/or numerical manipulations but does not have anything to do with the materials themselves.

A similar blister strength evaluation is conducted to estimate the performance of the FBE coatings towards the end of the design life. Similar assumptions of 60% decrease in surface contact mode-I fracture strength and 30% reduction in the Young's modulus of the coating materials were also done for this evaluation. The mode-I surface contact fracture strength is assumed to be 1.1kJ/m² for all three FBE coatings and the mode-II impact on the surface contact fracture strength is randomly taken as 0.3 for all cases. Figure 4.5 provides the estimated bounds of the maximum fluid pressure that can be stored underneath an osmotic blister with a radius of 5mm for all three FBE coatings.

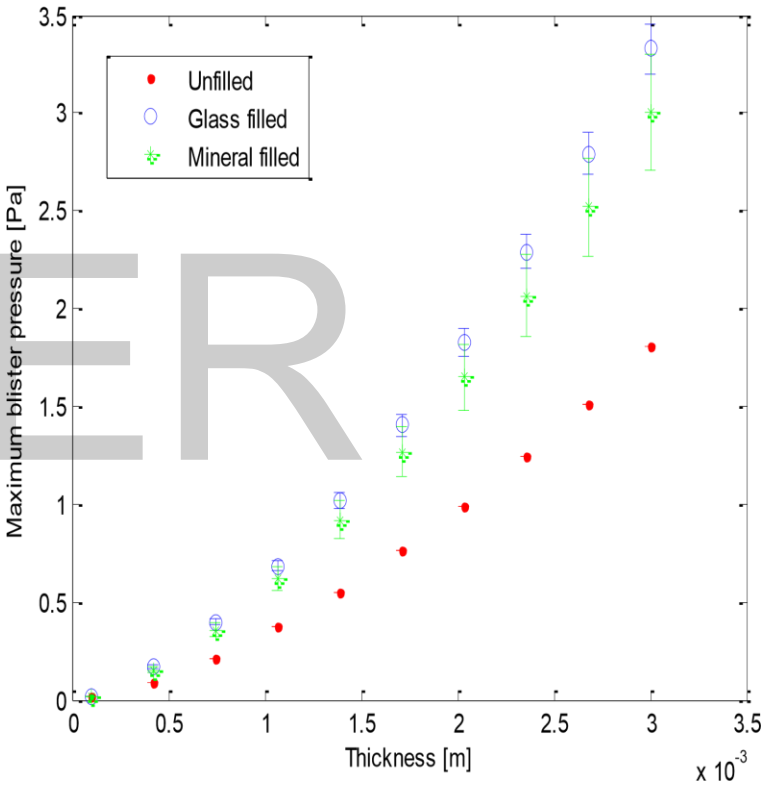

Figure 4.5: Comparative evaluation of the service life performance of the three FBE coatings based on later life blister evaluation

From Figure 4.5, the maximum allowable blister pressure for the FBE coating upon approaching its later life is observed to

INTERNATIONAL JOURNAL OF SCIENTIFIC & ENGINEERING RESEARCH, VOLUME 10, ISSUE 12, DECEMBER 2019
ISSN 2229-5518

be remarkably enhanced when fillers are added to the epoxy resin. It is observed that a glass filled FBE coating gives a better resistance to osmotic blistering in its later life than can be obtained with a mineral filled FBE coating. Taking into the consideration that the mineral filled epoxy gives an improved resistance to layer cracking as provided in Figure 4.4, the decision to use filler for the FBE coating may be subject to cost and/or technical limitations such as the needed resistance to chemical penetration, cathodic debondment and other forms of coating deterioration.

CONCLUSION

In this paper, a fundamental study of the importance of anticorrosive coatings to the long term protection of subsea systems was carried out. The work aimed to quantitatively evaluate the probability of failure of submerged single layer anticorrosive coatings, establish a design methodology to overcome where early coatings failed and demonstrate a performance based coating choice for long term corrosion protection of a coating system throughout the useful life of the protected system. These objectives were accomplished via analytical study of the fracture characteristics of bi-layered materials. Calculations based on fracture mechanics concepts were also done to analyze common failure modes of submerged anticorrosive coatings.

Fracture failure of the coating system as a result of channeling cracks on the coating layer, surface contact delamination and buckle driven debondment were considered in this study. The occurrence of each or a combination of these failure modes leads to decreased reliability and efficiency of the whole corrosion protection system for a subsea system. Thus, the design concept established was focused on mitigating all the earlier mentioned failure modes.

From the outcomes of this paper, it was discovered that coating layers and the surface contacts are more vulnerable to fast fracture with increasing thickness of the coating layer. The outcomes gotten for a fusion bonded epoxy coating used on steel were very much in harmony with the current industry approved practice for coating implementation. While the need for efficient resistance to osmotic blistering and mechanical buckling as a result of huge hydrostatic pressures require larger thicknesses for single layer coatings, it is proven that the susceptibility of the coating systems to fracture failures puts an upper limit on the allowable coating layer thickness.

This paper demonstrates the viability of the usage of the fracture mechanics for forecasting the mechanical failure of coating systems. More critically, it highlights the possibility of an integrated design concept to accomplish a long term

corrosion protection by coating systems on subsea structures.

REFERENCES

[1] National Association of Corrosion Engineers, 2002. NACE corrosion engineer's reference book. 3rd ed. Houston, Texas: NACE International.

[2] Det Norske Veritas, 2012. Risk based corrosion management. [Online]. Available at: www.dnvgl.com

[3] Satheesh Babu, P. K., Mathiazhagan, A. & Nandakumar, C. G., 2014. Corrosion Health Monitoring System for Steel Ship Structures. International Journal of Environmental Science and Development, 5(5), pp. 491-495.

[4] Det Norske Veritas, 2011. Factory applied external pipeline coatings for corrosion control. [Online]. Available at: www.dnvgl.com

[5] Bai, Y. & Bai, Q., 2005. Subsea pipelines and risers. 1st ed. Oxford: Elsevier Ltd.

[6] Joliff, Y., Belec, L. & Aragon, E., 2013. Influence of the thickness of pipeline coating on internal stresses during the manufacturing process by finite element analysis. Computational Material Science, Volume 68, pp. 342-349.

[7] Volinsky, A. A., 2006. Mechanical Aspects of Anti-Corrosive Coatings Performance Tests. San Diego, California, NACE International.

[8] Mitchell, M. J., Claydon, D. & Ward, D., 2005. A Critical Review of Current Performance Tests for Offshore Anti-corrosive Coatings. Houston, Texas, NACE International.

[9] Evans, A. G. & Hutchinson, J. W., 1995. The thermomechanical integrity of thin films and multilayers. Acta Metallurgica et Materialia, 43(7), pp. 2507-2530.

[10] Suo, Z. & Hutchinson, J. W., 1990. Interface crack between two elastic layers. International Journal of Fracture, Volume 43, pp. 1-18.

[11] Hutchinson, J. W. & Suo, Z., 1991. Mixed mode cracking in layered materials. Advances in applied mechanics, Volume 29, pp. 63-191.

[12] Wan, K.-T. & Mai, Y.-W., 1995. Fracture mechanics of a new blister test with stable crack growth. Acta Metallurgica et Materialia, 43(11), pp. 4109-4115.

[13] Sue, H.-J. & Chang, B. T. A., 2006. External pipeline coating integrity –One Year Extension (DTPH56-06-T-000022). [Online] Available at: https://primis.phmsa.dot.gov/matrix/PrjHome.rdm?prj=206

[14] Lau, D., 2011. Moisture-induced debonding in concrete-epoxy interface. The Hong Kong Institution of Engineers Transactions, 19(3), pp. 33-38.

[15] Lima, C. R. C., Suoza, N. F. C. & Camargo, F., 2013. Study of wear and corrosion performance of thermal spray engineering polymers. Surface and Coatings Technology, Volume 220, pp. 140-143.

[16] CES EduPack '18, 2018. Material Universe. United Kingdom: Granta Design.

[17] Perera, D. Y., 1996. On adhesion and stress in organic coatings. Progress in Organic Coatings, Volume 28, pp. 21-23.

[18] Anderson, T. L., 2005. Fracture mechanics: fundamentals and applications. 3rd ed. Boca Raton: CRC Press.